Simulating RFP and Spheromak Relaxation with Thermal Transport

Carl Sovinec and Fatima Ebrahimi,
University of Wisconsin-Madison

Bruce Cohen and Simon Woodruff,
Lawrence-Livermore National Laboratory

Eric Held,
Utah State University

Innovative Confinement Concepts Workshop
January 22-24, 2002
College Park, Maryland

Motivation

Nonlinear simulations of the RFP and spheromak using the zero-beta MHD model have provided important information on the role of three-dimensional current-driven activity in each of these configurations. Equally significant insight on the role of pressure-driven activity is expected from simulations with finite-beta models. However, since relaxation occurs on time scales that are comparable to energy transport, closures normally used for MHD analysis are inadequate. Three-dimensional modeling has to account for the extreme anisotropy of transport processes with respect to the magnetic field direction.

Objectives

- To learn about the confinement properties of magnetic configurations with global MHD fluctuations that produce relaxation.

- To understand the role of pressure-driven modes in these configurations.

Outline

I. Modeling
   A. Equations
   B. Numerical accuracy
   C. Kinetic heat flux

II. Reversed-field pinch studies
   A. Characterizing linear pressure-driven modes
   B. Nonlinear simulations

III. Finite-β SSPX spheromak studies

IV. Summary and future work

Modeling

Equations—Nonideal MHD+

$$\frac{\partial \mathbf{B}}{\partial t} = -\nabla \times \mathbf{E}$$

$$\mathbf{E} = -\mathbf{V} \times \mathbf{B} + \eta \mathbf{J}$$

$$\mu_0 \mathbf{J} = \nabla \times \mathbf{B}$$

$$\frac{\partial n}{\partial t} + \nabla \cdot (n\mathbf{V}) = \nabla \cdot D \nabla n$$

$$\rho\left(\frac{\partial \mathbf{V}}{\partial t} + \mathbf{V} \cdot \nabla \mathbf{V}\right) = \mathbf{J} \times \mathbf{B} - \nabla p - \nabla \cdot \nu\rho \nabla \mathbf{V}$$

$$\frac{n}{\gamma - 1}\left(\frac{\partial T}{\partial t} + \mathbf{V} \cdot \nabla T\right) = -p \nabla \cdot \mathbf{V} - \nabla \cdot \mathbf{q} + Q$$

- Version 3_1 of the NIMROD code [http://nimrodteam.org] solves this set of equations, where **q** represents anisotropic conductive heat flux: $\mathbf{q} = -n\left[\chi_{\parallel}\hat{\mathbf{b}}\hat{\mathbf{b}} + \chi_{\perp}\left(\mathbf{I} - \hat{\mathbf{b}}\hat{\mathbf{b}}\right)\right] \cdot \nabla T$ and Q is the sum of Ohmic and viscous heating.
- Separating ion and electron temperatures and a thermal equilibration term are available.
- Work on kinetic electron heat flux is described below.
- Two-fluid modeling capabilities are under development.

Numerical Accuracy

- Nonlinear simulations of high-temperature plasmas must be able to resolve thermal transport anisotropy associated with the magnetic field direction.
  - The saturation of pressure-driven modes is sensitive to changes in magnetic topology due to parallel thermal conduction.
  - The ratio of parallel to perpendicular thermal conductivities leads to one threshold mechanism for neoclassical tearing modes.
- When the magnetic field is aligned with the grid or when the angle between $\hat{\mathbf{b}}$ and the grid is uniform, the anisotropy is accurately represented by standard techniques.
- A nonlinearly evolving magnetic topology requires more sophisticated approaches:
  - There is curvature in the magnetic field.
  - The topology of islands and stochastic regions is three-dimensional.
  - Even 3D automated mesh refinement schemes would be severely challenged by these conditions; 3D refinement is possible but 3D alignment near a separatrix is not.
- The **NIMROD** code has addressed this challenge by using high-order finite-element basis functions, which represent curvature with or without alignment.
  - The increase in spatial convergence rates with basis function order has been verified.
  - Spatial convergence rates are retained with nonuniform meshing.

A quantitative measure of the numerical error can be determined by a simple test problem.

- The simplest thermal conduction problem is a 2D box with Dirichlet boundary conditions and a source. If the source drives the lowest eigenfunction only,

  $$S(x,y) = 2\pi^2 \cos(\pi x)\cos(\pi y)$$

  in the domain

  $$-0.5 \le x \le 0.5, -0.5 \le y \le 0.5 \ ,$$

  it produces the temperature distribution

  $$T(x,y) = \kappa^{-1} \cos(\pi x)\cos(\pi y) \ .$$

- A numerical test with **B** everywhere tangent to this temperature distribution and a uniform rectilinear grid has $\hat{\mathbf{b}}$ severely misaligned with the grid. With $\kappa_\perp = 1$ and $\kappa_{||} >> 1$, the inverse of the resulting $T(0,0)$ is a good measure of the effective $\kappa_\perp$ of the numerical algorithm.

- The magnetic field is created by inducing a perpendicular current density distribution that is proportional to the heat source.

Results from the Anisotropic Diffusion Test

Effective κ_{perp}-1 for $\kappa_{||} = 10^3$

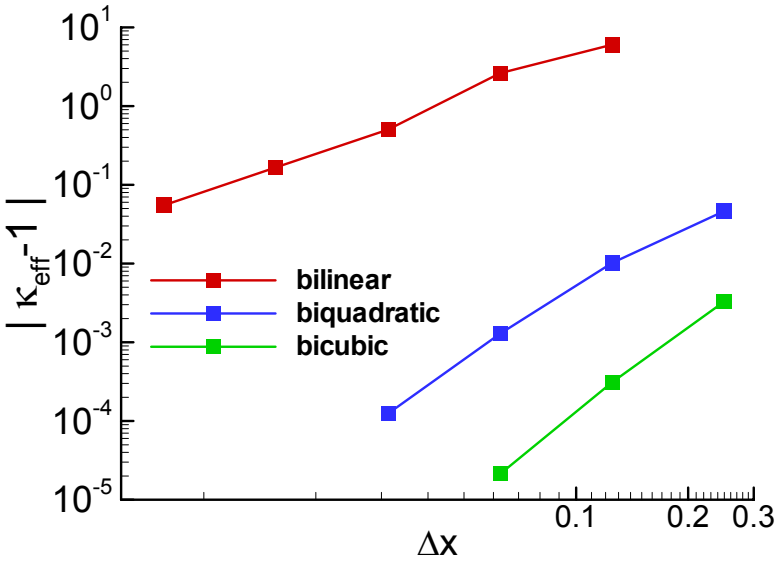

Effective κ_{perp}-1 for $\kappa_{||} = 10^6$

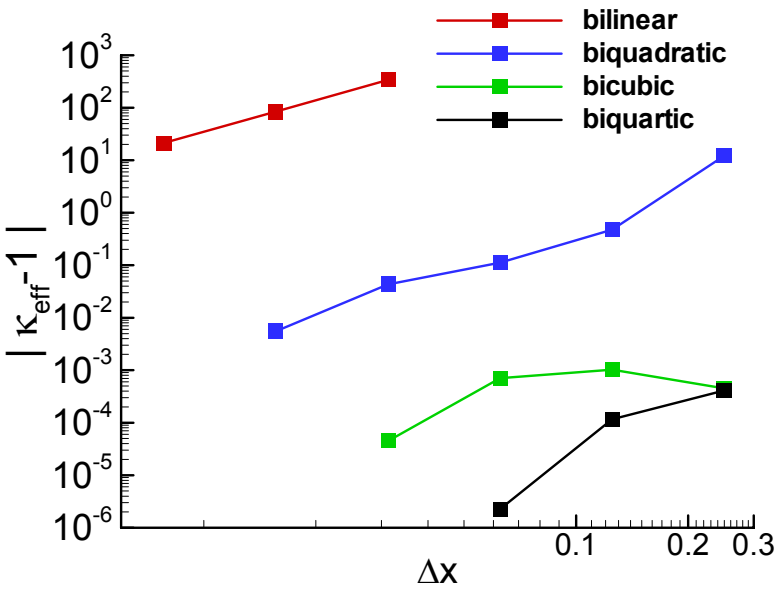

Effective κ_{perp}-1 for $\kappa_{||} = 10^9$

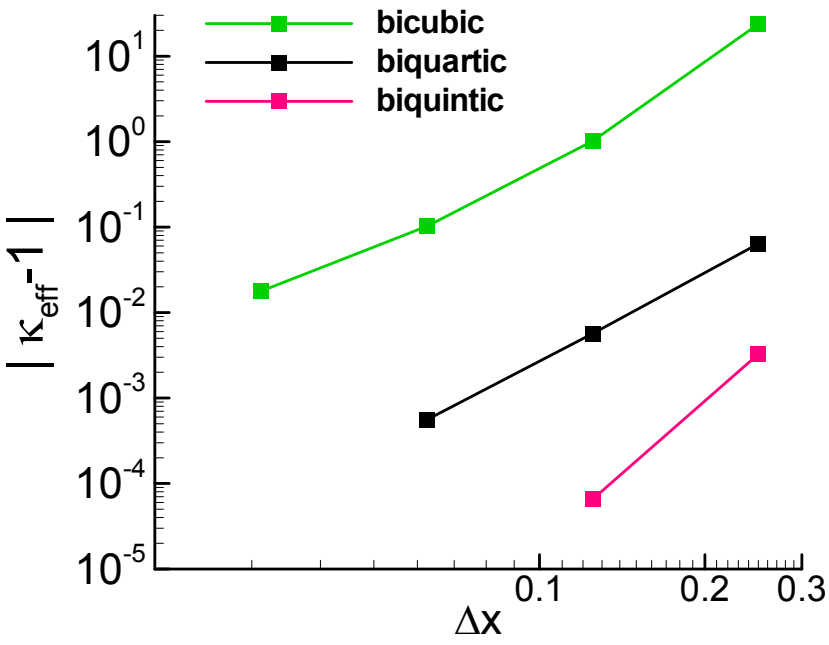

High-order basis functions enable resolution of extreme anisotropy in nonlinear simulations of electromagnetic fusion physics.

Finite elements also provide geometric flexibility.

These NIMROD features are making a wide range of tokamak and alternates simulations possible.

Anisotropic Diffusion Demonstration

- Start from a saturated island in a DIII-D-like equilibrium.
- Freeze magnetic evolution and just run anisotropic thermal diffusion over the perpendicular time-scale (100 x resistive time-scale).
- $\kappa_\perp$=0.423, $\kappa_\parallel$=4.23x10^{8}, Δt=1x10^{-4} s. 48x28 packed bicubics.
- Island appears in pressure contours immediately.

Pressure contours (color) after 1.5 ms of anisotropic diffusion overlaid with Poincare surface of section.

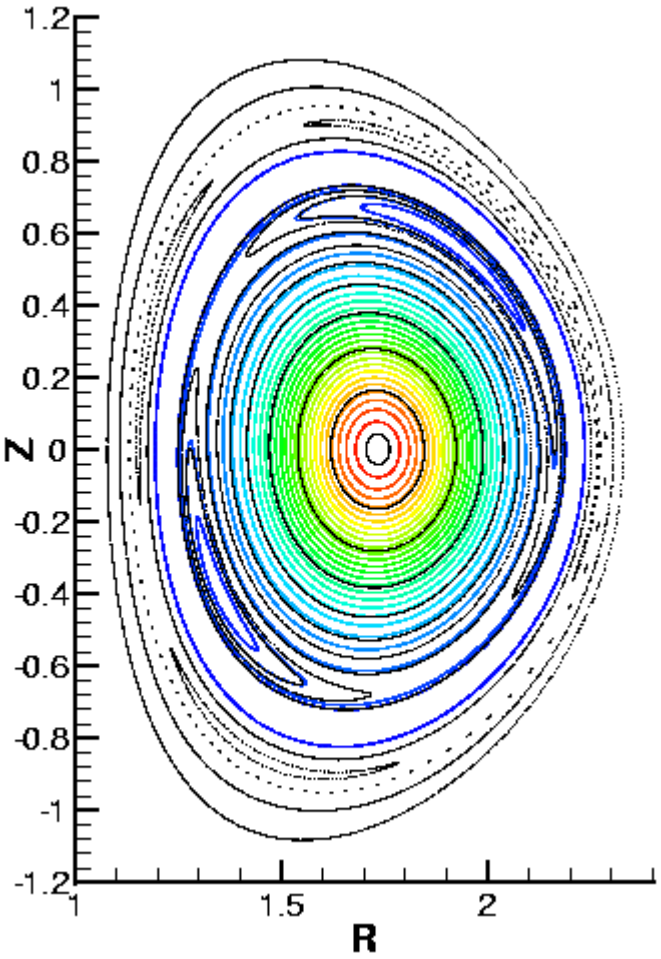

Kinetic Heat Flux

The collisional form of heat conduction is not valid at the parameters of laboratory experiments, though we expect it can be useful in simulations if $\chi_{\|}$ is calibrated to achieve realistic temperature profiles. A first-principles calculation must account for the large effective mean free path of electrons. A method of calculating heat flux at arbitrary collisionality is being developed for this purpose [Held, *et al.*, PoP 1171 (2001)].

- Solve the electron drift kinetic equation with a Chapman-Enskog-Like (CEL) approach. Expansion is based on drift ordering, not collisionality, but the lowest-order solution is the Maxwellian distribution.
- Velocity-space distortions from the local Maxwellian are expanded in Legendre polynomials in pitch angle (eigenfunctions of the Lorentz scattering operator).
- Solutions then lead to algebraically coupled integral forms:

$$F(s,\xi,L') = \sum_{n=1}^{N} P_n \sum_{\bar{k}_i>0} a_{ni} \int_0^{\infty} dl \left(g(L'+L)+g(L'-L)\right) e^{-\int_0^{\infty} d\bar{L}\,\bar{k}_i}$$

  where $\bar{k}_i^{-1}$ is a speed-dependent effective mfp, and g describes parallel gradients of the Maxwellian.
- Integrals to determine $q_{\|}$ are carried out along individual magnetic field line trajectories until convergence.
- Parallel computing makes this possible in 3D simulations.

For an RFP, magnetic field-line wandering is large enough to sample essentially the entire cross section within the convergence distance of the heat flux integral.

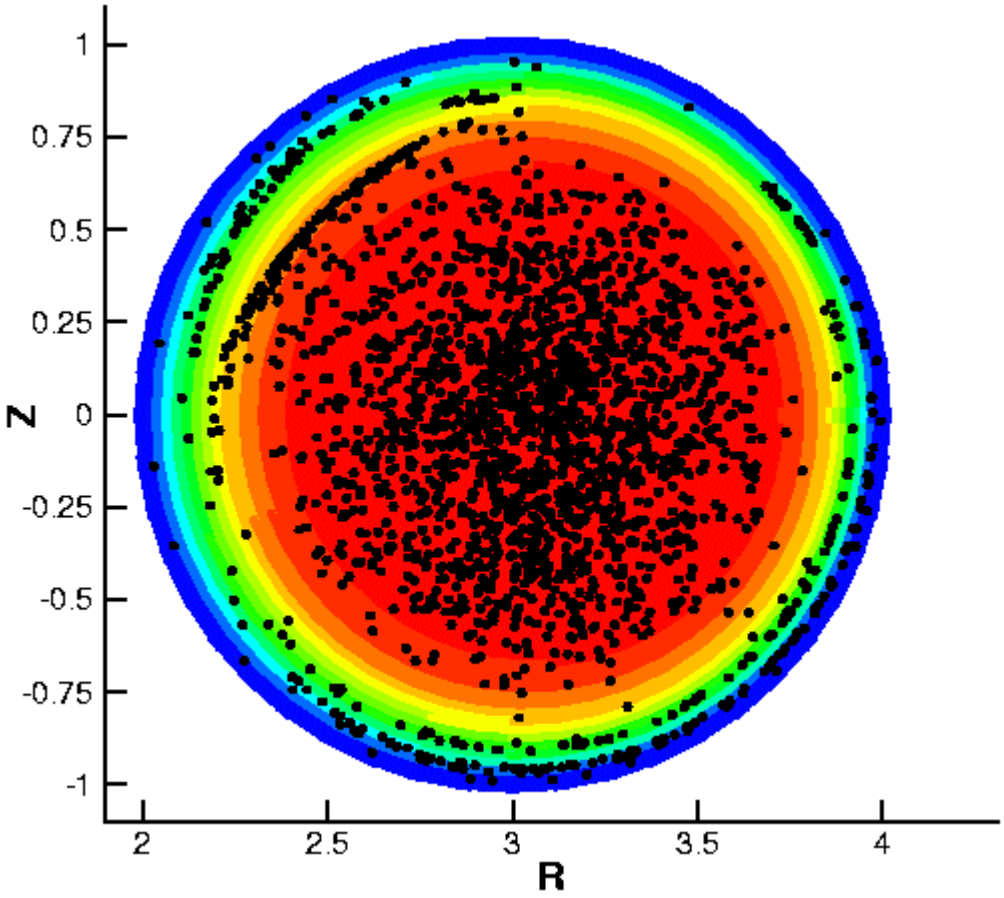

Magnetic field line puncture plot (not representative of convergence distance) superposed on temperature contours.

Effective local values of $\chi_{<\psi>}$ can be negative, indicating heat flowing against the local temperature gradient due to long-range effects.

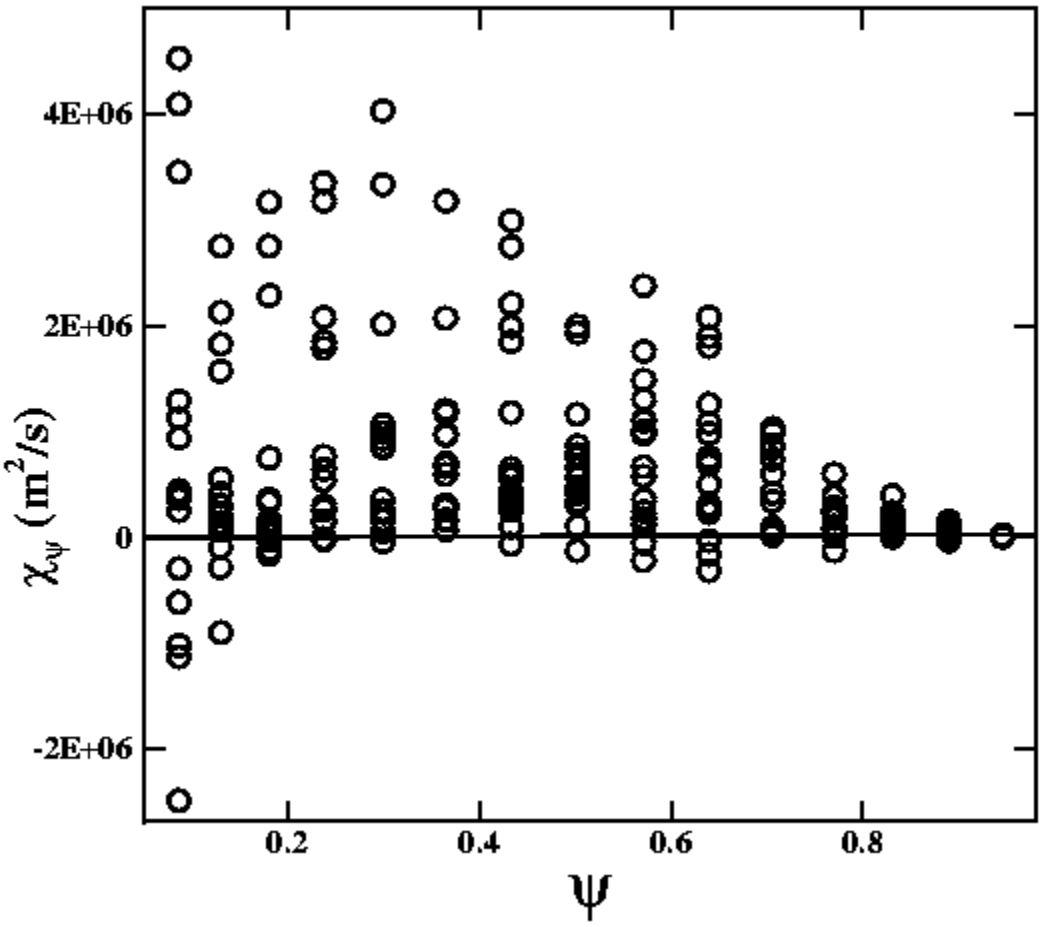

Variations in |B| along individual field-lines are significant. The double-well modulations result from poloidal transits plus radial wandering.

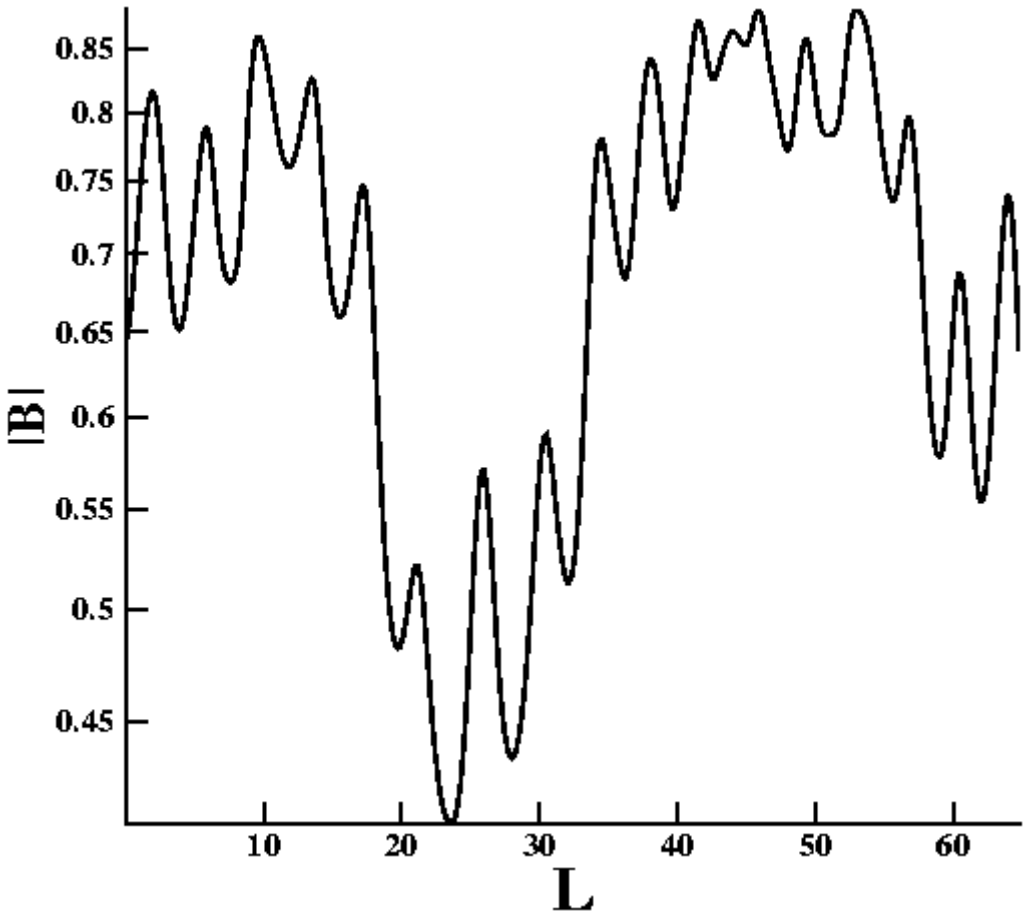

Including the trapping effects is essential. Sample kinetic calculations of effective radial conductivity show order-of-magnitude changes with conservative estimates for |B|-variation.

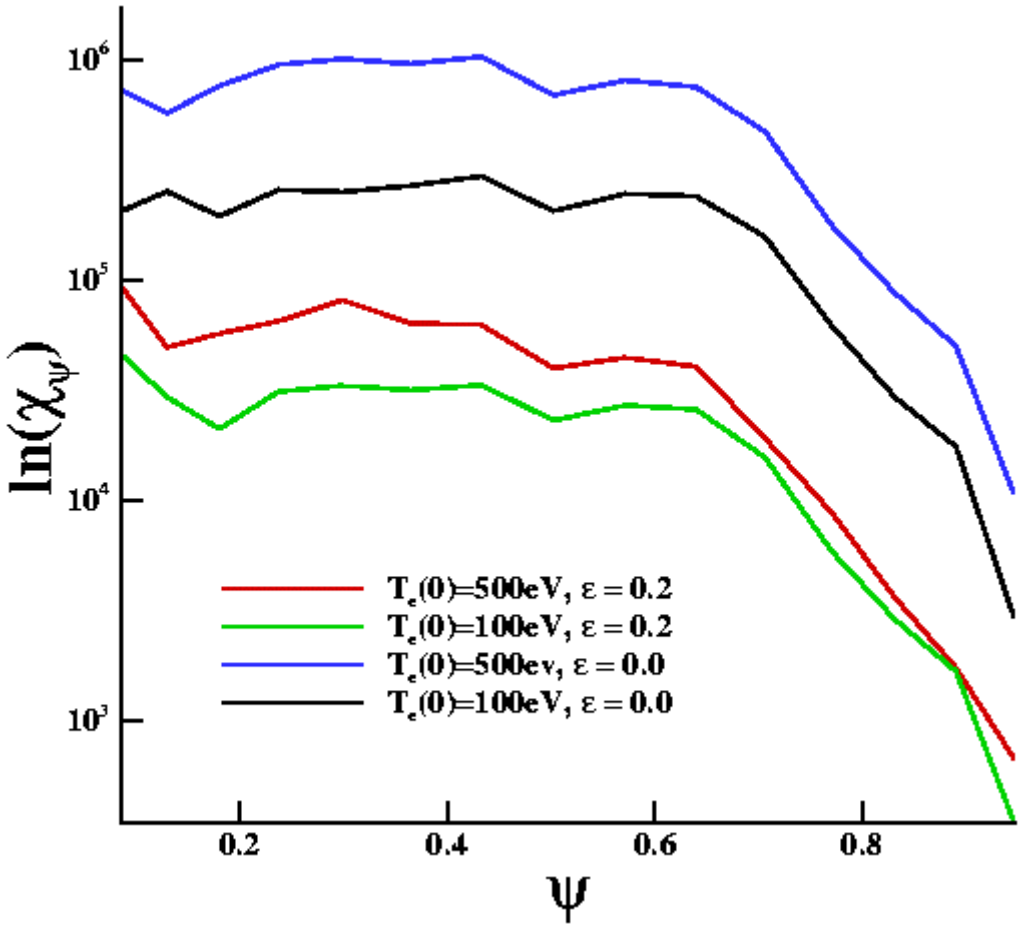

Reversed-Field Pinch Studies

Characterizing Linear Pressure-Driven Modes

The role of pressure in driving fluctuations may have more relative importance in RFP experiments with Pulsed Poloidal Current Drive (PPCD) and in future experiments with noninductive profile control, since the current drive is reduced. Linear calculations are being used to benchmark finite pressure simulations and to explore conditions at high beta, where modes transition to ideal behavior.

- We have used the nonlinear DEBS code [Schnack, *et al.* JCP '87] to perform calculations in the linear regime with an adiabatic pressure equation.
- Profiles have $\Delta' < 0$, and are therefore stable at zero β.
  $\lambda(r) = 2\Theta_0\left(1 - r^{\alpha}\right), \qquad p(r) = p_0\left(1 - 0.9\, r^{\delta}\right)$
- $\Theta_0 = 1.6, \quad \alpha = 4, \quad \delta = 3$
- High-k calculations have m=1, k=10.5.
- Low-k calculations have m=1, k=1.8.

For high-k and realistic S-values, the transition to ideal behavior occurs at large D_s-values (> Suydam criterion of ¼).

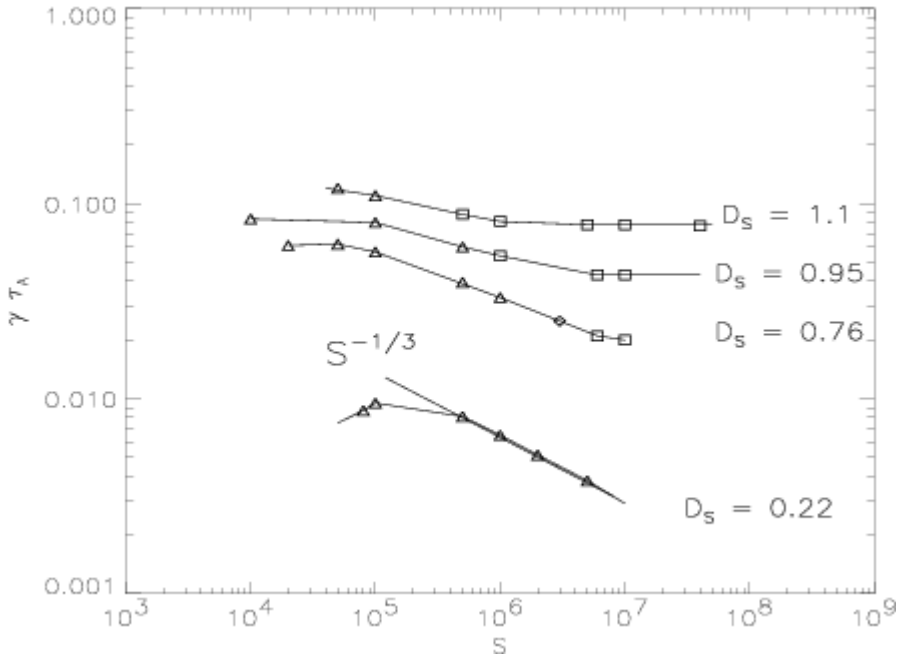

The shape of $|b_r|$ for the eigenfunction confirms the transition.

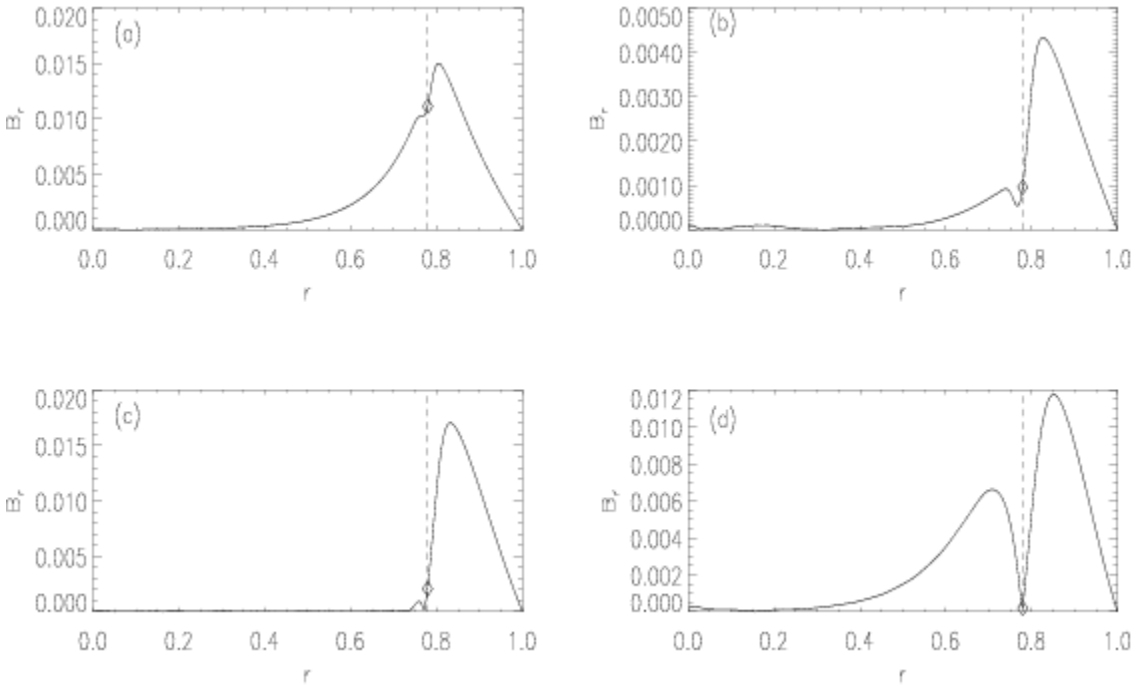

S=10^6, a) D_s=0.23, b) D_s=0.76, c) D_s=0.95, d) D_s=1.72.

Low-k modes also have a transition. ($S=10^4$ and 10^5).

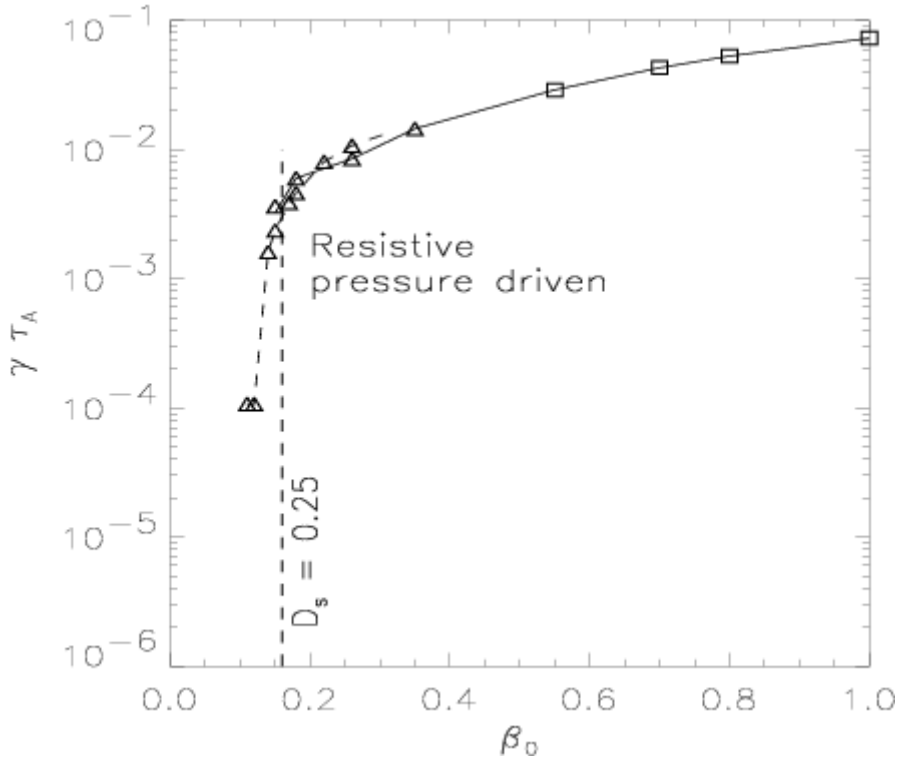

Eigenfunctions appear similar to zero-β tearing modes at low D_s, transitioning to nonconstant-ψ and kink behavior at high D_s.

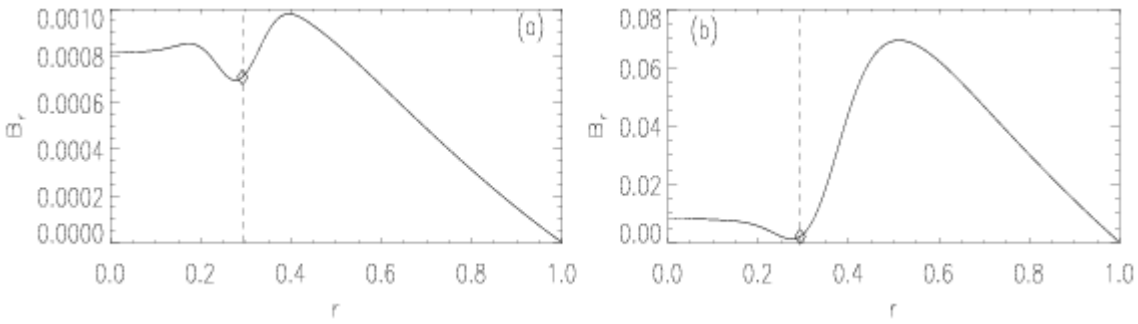

Nonlinear Simulations

We are performing preliminary nonlinear RFP simulations with NIMROD to verify functionality of number density and temperature evolution with anisotropic conduction.

- Toroidal geometry, R/a=1.75, S=2x10^4, Pm=10.
- $\chi_{\|}/\chi_{\perp} = 10^4$; magnitudes chosen to result in realistic final β with thermal transport from $\left\langle \tilde{q}_{\|} \tilde{b}_{\psi 00} \right\rangle$.
- The value of D is based on particle confinement times from experiment, scaled relative to relaxation processes.
- Started from a β=0 simulation. Internal energy builds from Ohmic and viscous heating (mostly Ohmic).

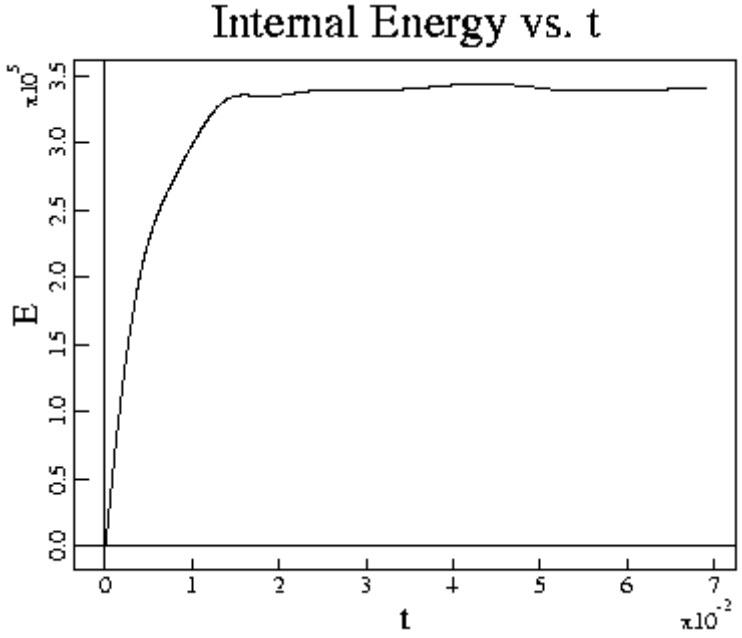

Time is in diffusion times. Resulting $\tau_E \cong 6 \times 10^{-3}$.

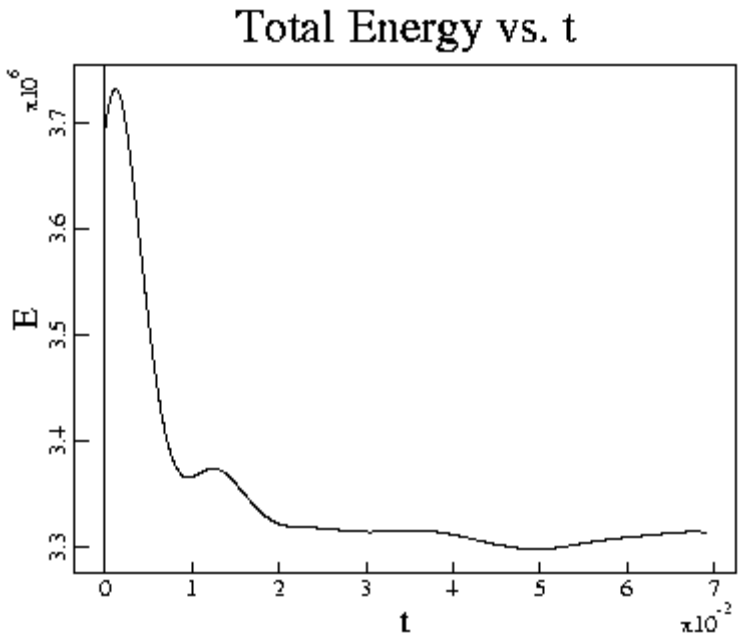

- Reversal parameter diagnostic shows that toroidal field remains reversed. Simulations resulting in large β-values tend to lose reversal at this pinch parameter (Θ=1.6).

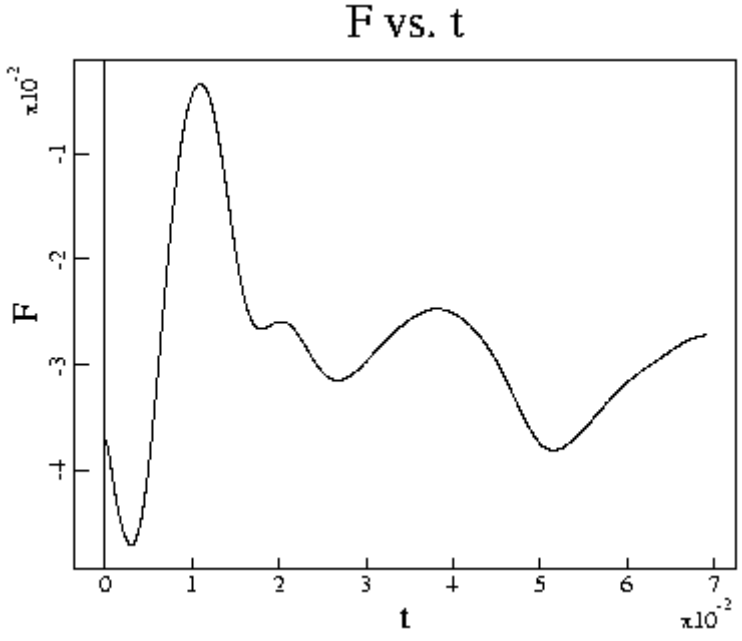

- A comparison of the magnetic and kinetic fluctuation spectra from zero to finite-β conditions shows little change in $\int \tilde{b}^2$, whereas $\int \rho \tilde{v}^2$ increases significantly.

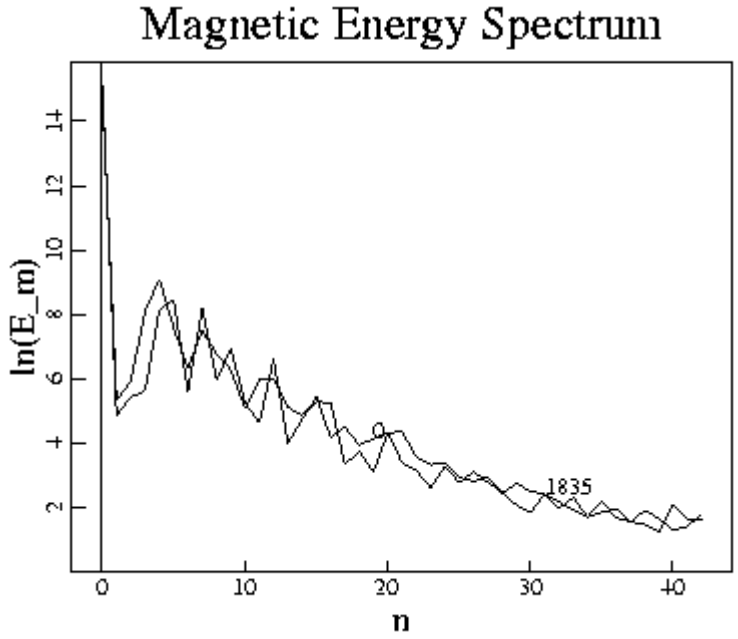

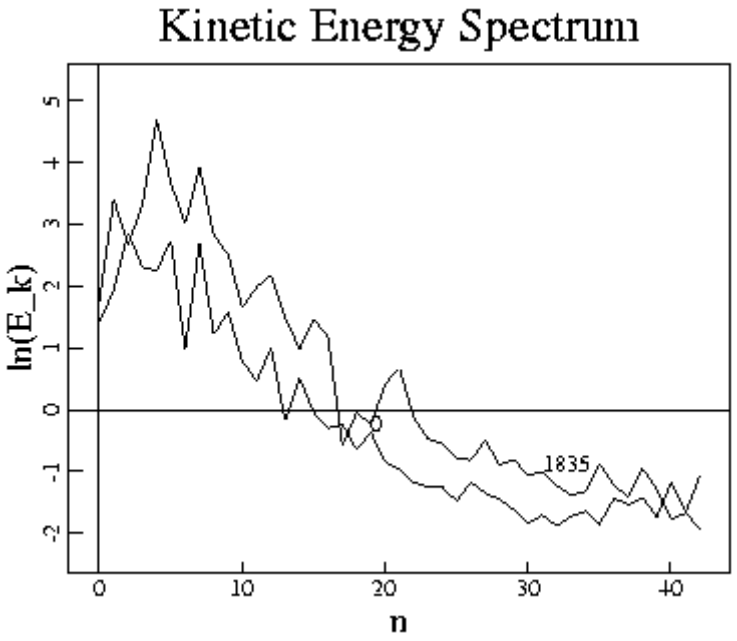

Spectra labels indicate time-step: "0" is the initial state (0-β), "1835" is the final (β~11%) state.

- The resulting n=0 density and temperature profiles are fairly flat in the interior. Density variation (due to pinching) is small (~25%).

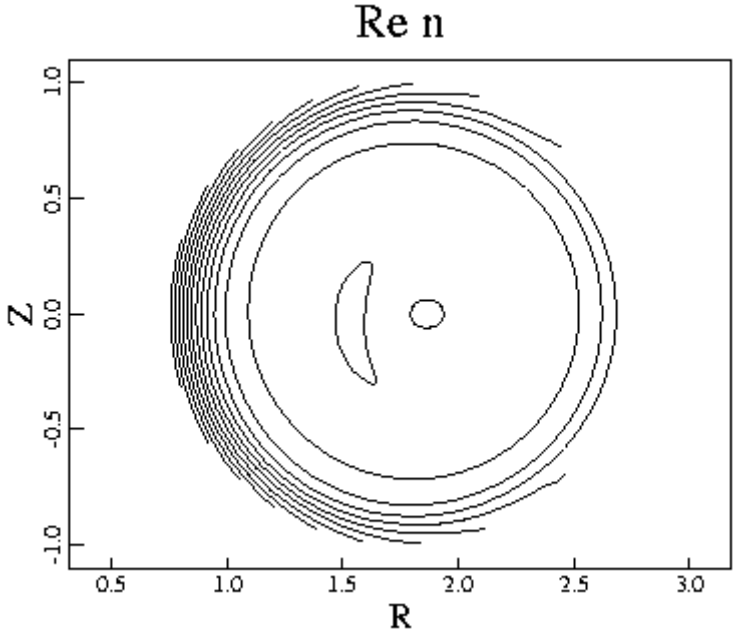

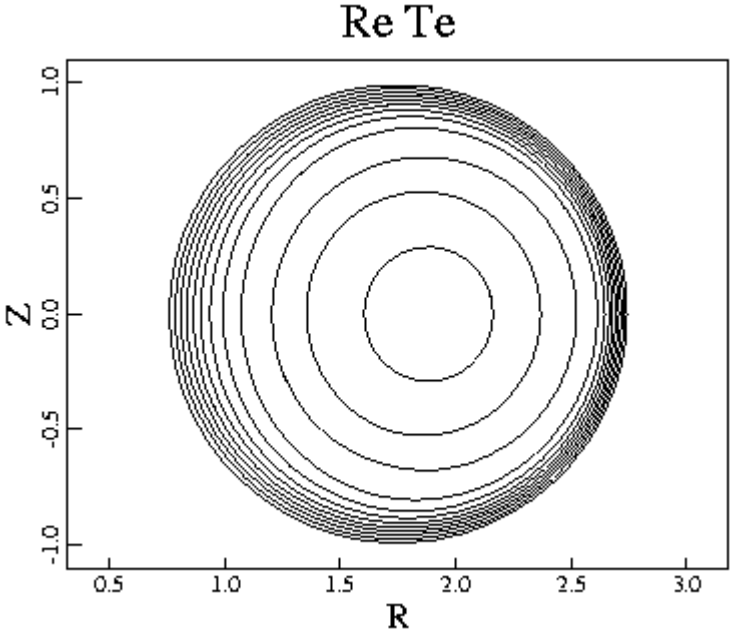

- The toroidal simulation uses only the *n*=0 part of number density in inertia and thermal conduction terms. The following results from cylindrical geometry, S=2000 simulations compare this approximation against using the full 3D number density in these terms. [The continuity equation is unchanged (always 3D).]

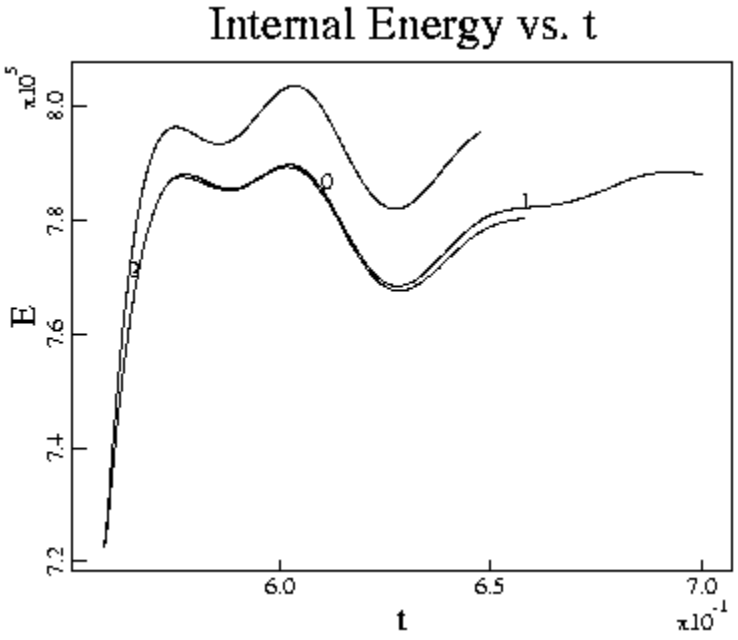

Trace "0" uses the full continuity option, trace "1" uses *n*=0 in the coefficient, and trace "2" is a higher resolution version of "1".

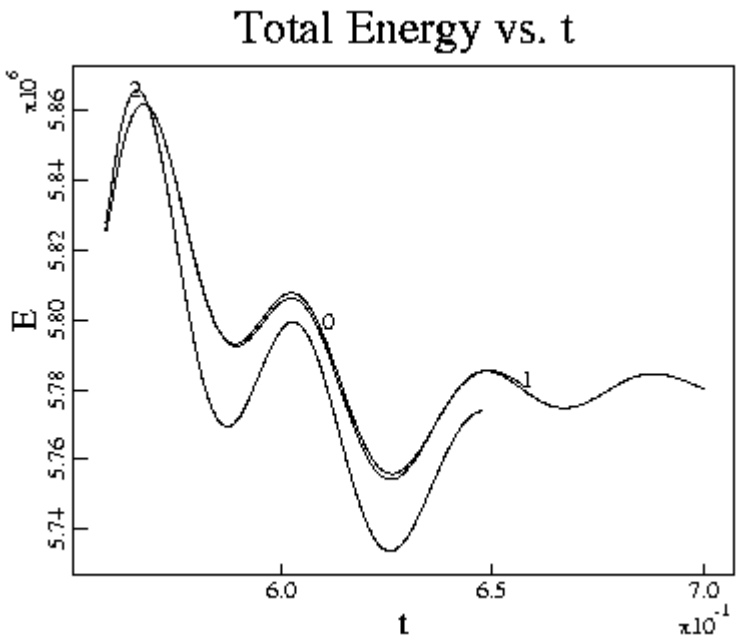
Total Energy vs. t
E
x10^6
5.86
5.84
5.82
5.80
5.78
5.76
5.74
2
0
1
6.0
6.5
7.0
t
x10^-1

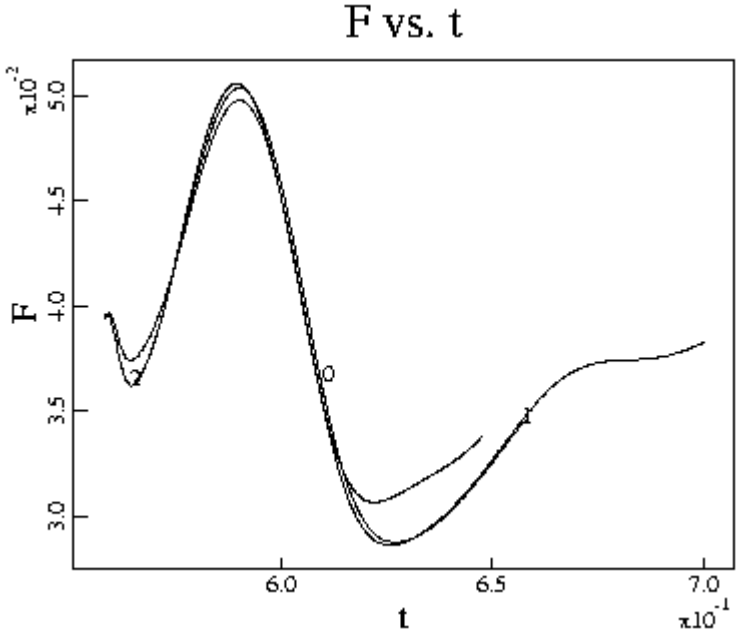
F vs. t
F
x10^-2
5.0
4.5
4.0
3.5
3.0
2
0
1
6.0
6.5
7.0
t
x10^-1

Finite-β SSPX Spheromak Studies

Zero-β simulations of SSPX formation qualitatively and semi-quantitatively agree on many features:

- Typical magnetic flux amplifications O(1.5-2.5)
- Strongly driven (by axisymmetric electrostatic fields) spheromak formation is mediated by an n=1 resistive tearing instability
- Expected spheromak magnetic field structures are observed:
- Safety factor q vs. r, $\lambda = \mu_0 \vec{J} \cdot \vec{B} / \vec{B} \cdot \vec{B}$ vs. r, B_{tor}, B_{pol} vs. x,y
- Decaying plasmas see a decrease in n=1 and harmonic perturbation amplitudes leading to improved magnetic field structures (including the emergence of closed field lines)
- Decaying plasmas with peaked current profiles can see n=2 modes

Finite-β simulations are underway, and the results so far merit further investigation:

- Simulations with finite pressure see electron β_{peak}~3-8% with relatively weak dependence on the plasma density over a range of 10^4 in density.
- Simulations with increasingly realistic parameters (e.g., densities and temperature-dependent resistivities) are being performed.

SSPX Observes β_e= 1- 7% vs. NIMROD β_e= 6 - 8%

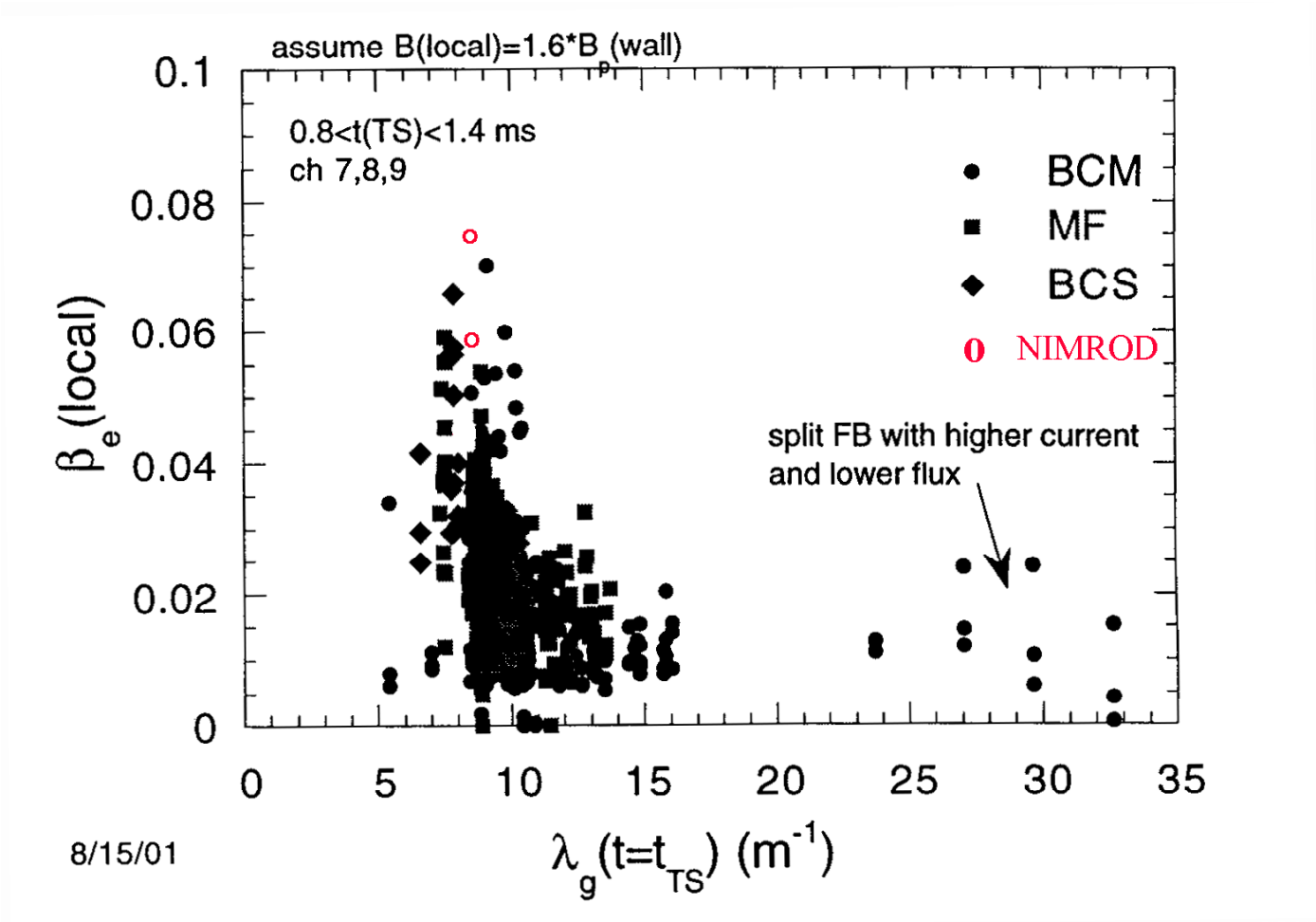

NIMROD simulations are at two different thermal conductivities: κ=10^2 & 10^4.

NIMROD Simulation of SSPX -- q and λ Profiles

- NIMROD profiles of q and λ are similar to CORSICA reconstructions based on edge field measurements:

NIMROD

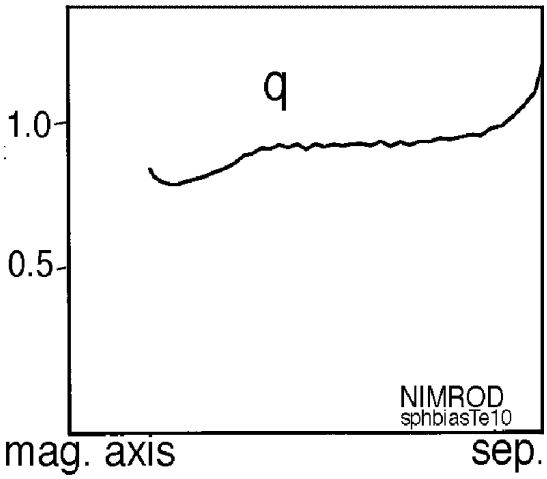

NIMROD

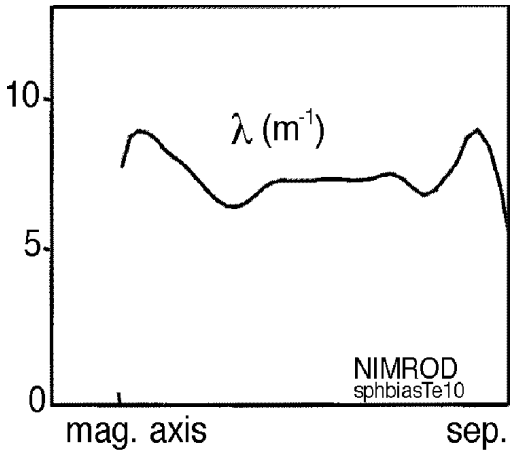

CORSICA + SSPX

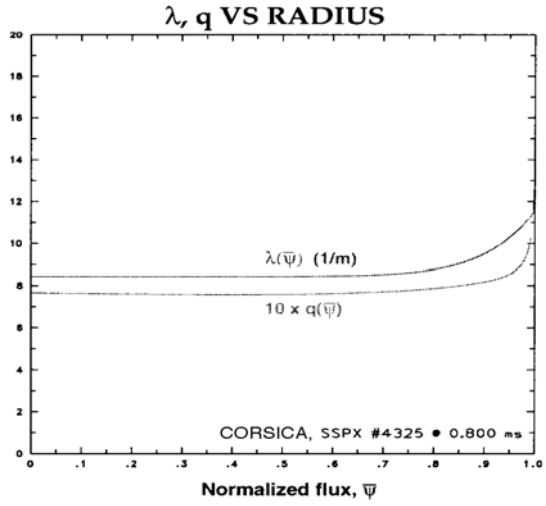

NIMROD SSPX Simulations with Finite Pressure See β_e=6-15%

- NIMROD simulations with finite pressure include Ohmic heating, isotropic thermal conduction, and classical electron resistivity $\propto T_e^{-3/2}, T_e \geq 5eV$

$$\frac{3}{2}\left(\frac{\partial}{\partial t}+\vec{v}\cdot\nabla\right)P = -P\nabla\cdot\vec{v}+\kappa\nabla^2 P+\eta J^2 \quad \text{(pressure eqn.)}$$

$$\vec{E}+\vec{v}\times\vec{B}=\eta\vec{J} \quad \text{(Ohm's law)}$$

$$\rho\left(\frac{\partial}{\partial t}+\vec{v}\cdot\nabla\right)\vec{v} = -\nabla P+\vec{J}\times\vec{B}+\rho\nabla\cdot(\nu_{vis}\nabla\vec{v}) \quad \text{(mom. eqn.)}$$

- The observed peak $\beta_e = 2\mu_0 P/B^2$ values in the driven steady states have a very weak dependence on plasma density (held constant in these simulations) for fixed driving electric field 100V/m, and the temperature profile exhibits some peaking. Note that the pressure and Ohm's law equations have no direct dependence on density, which primarily affects the inertia in the flows.

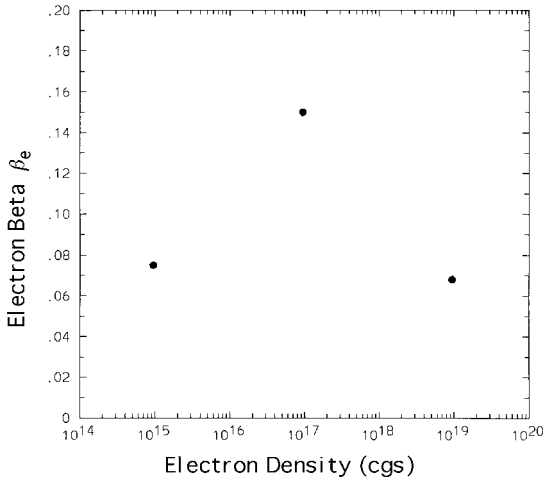

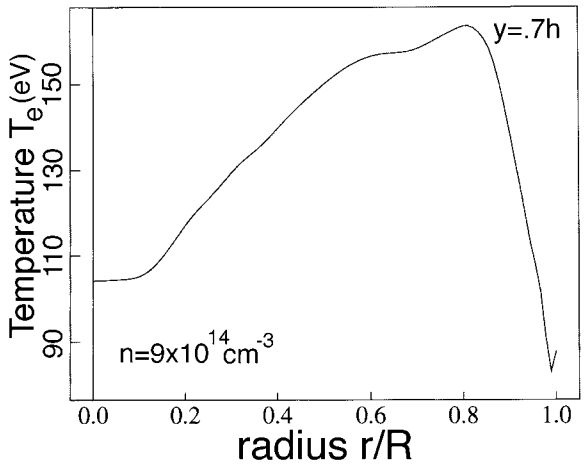

NIMROD SSPX Simulations of SSPX with Finite Pressure (cont'd)

- The simulations are demonstrating the potential importance of convection and compression:

$\frac{3}{2}(\frac{\partial}{\partial t}+\vec{v}\cdot\nabla)P=-P\nabla\cdot\vec{v}+\kappa\nabla^2P+\eta J^2$ pressure equation

|----------1---------| |---2---| |--3--|

(1)convection/compression (2)thermal conduction (3)Joule heating

- Compare two simulations with n_e=9.5x10^{20}m^{-3}, E_0=100V/m, bias coils, and different initial temperatures and thermal conductivities:

sphbiasTe10a: κ=10^2 $T_e(0)$~100eV

sphbiasTe15: κ=10^4 $T_e(0)$~100eV

Both evolve to similar final states with $\beta=2P/(B^2/\mu_0)\sim 6-7\%$ and $T_e\sim 100-150eV$ with convection and compression dominant over thermal conduction and Joule heating at t~2 ms.

Simulation	convection/ compression	thermal conduction	Joule heating
sphbiasTe10a	2x10^8	8x10^6	4x10^7
sphbiasTe15	2x10^9	8x10^8	1x10^8

NIMROD SSPX Simulations of SSPX with Finite Pressure (cont'd)

- Consider a simulation with n_e=9.5x10^{20}m^{-3}, E_0=1500V/m, bias coils, initial temperature ~0.1 eV and thermal conductivity κ=10^6 and η =10^{-4} (sphbiasTe18).
- Because of the high thermal conductivity, this simulation evolves to a low T_e~0.6eV (peak), with Joule heating balancing thermal conduction at t~4ms:

convection/ compression	thermal conduction	Joule heating
~2x10^6	~4x10^8	10^8-10^9

NIMROD SSPX Simulations of SSPX with Finite Pressure (cont'd)

- The peak β~2.5x10^{-4}, and the pressure profile is smooth. The steady-state temperature is sensitive to the numerical values of (and, in the experiment, the temperature dependences of) both η and $\vec{\kappa}$.

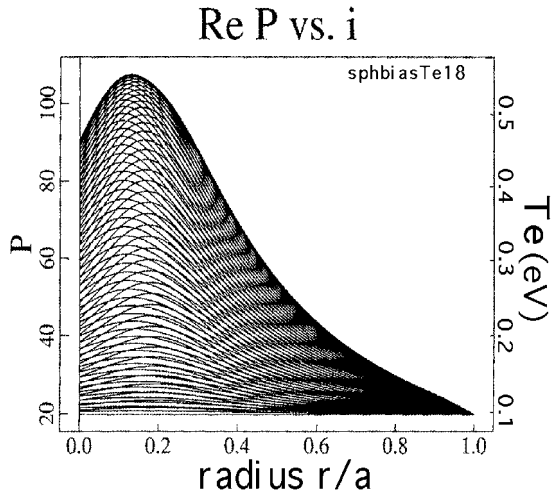

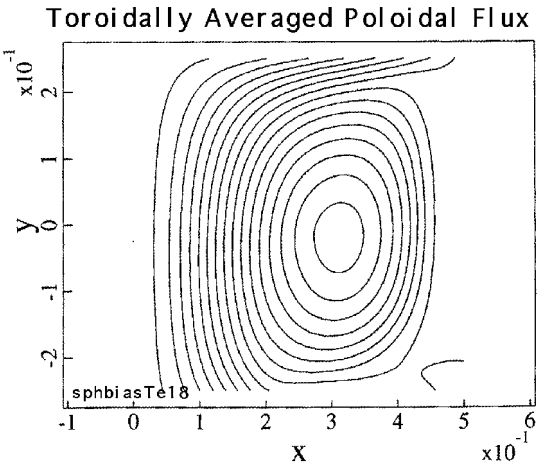

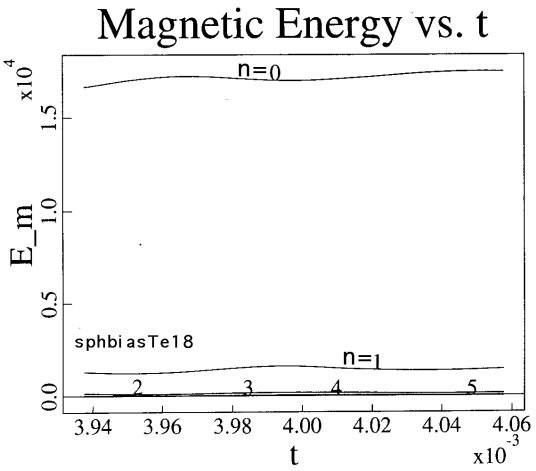

Conclusions and Future Work

- The spatial accuracy required to simulate the extreme anisotropy of plasma heat flux is available with high-order finite element representation.
- CEL calculations of kinetic electron heat flux are being developed, and they are suitable use in parallel simulations. Effects due to |B|-variations are essential.
  - Analytic work to capture these effects is underway in parallel with numerical implementation in NIMROD for use in time-dependent simulations.
- Linear calculations of pressure-driven modes for RFP profiles show transition from resistive to ideal behavior at D_s-values much larger than the Suydam criterion.
- Nonlinear simulations of RFPs with density and temperature evolution are possible with NIMROD. Simplifying coefficients by ignoring nonsymmetric variations in density seems to preserve accuracy.
  - Studies will explore the role of pressure-driven effects in standard and profile-control operating conditions.
- Nonlinear NIMROD simulations of the SSPX spheromak indicate that compressive heating may be significant at high temperature, whereas Ohmic heating is significant at lower temperature.
  - Including anisotropic heat flux will address confinement issues with open field line configurations.